https://doi.org/10.31925/farmacia.2026.3.15 **ORIGINAL ARTICLE**

IN VITRO INSIGHT INTO THE POTENTIAL OF CURCUMIN TO ENHANCE THE SENSITIVITY OF A375 HUMAN MELANOMA CELLS TO CISPLATIN

RALUCA-ANDREEA JUPÂNEANȚ [1,2,#], ALINA ANTON [3,4,#], MARINELA BOJINCĂ [1]*, DIANA HAJ ALI [1,3,4], IASMINA-ALEXANDRA PREDESCU [1,3,4], ANDRA TIBERIA PĂCURAR [1,3,4], DALIBORCA VLAD [2], VICTOR DUMITRAȘCU [2], ANDRADA IFTODE [3,4]

[1]Doctoral School, "Victor Babeș" University of Medicine and Pharmacy, 2 Eftimie Murgu Square, 300041, Timișoara, Romania
[2]Biochemistry and Pharmacology Department, Discipline of Pharmacology, Faculty of Medicine, "Victor Babeș" University of Medicine and Pharmacy, 2 Eftimie Murgu Square, 300041 Timișoara, Romania
[3]Research Centre for Pharmaco-Toxicological Evaluations, "Victor Babeș" University of Medicine and Pharmacy, 2 Eftimie Murgu Square, 300041, Timișoara, Romania
[4]Department of Toxicology, Drug Industry, Management and Legislation, Faculty of Pharmacy, "Victor Babeș" University of Medicine and Pharmacy, 2 Eftimie Murgu Square, 300041, Timișoara, Romania

**corresponding author: marinela.bojinca@umft.ro*
[#]Authors with equal contribution.

Manuscript received: February 2026

Abstract

Melanoma is one of the most aggressive and deadly forms of skin cancer, and despite recent therapeutic advances, treatment efficacy is often limited by drug resistance and unsatisfactory safety profiles. Therefore, increasing attention has been directed toward alternative approaches to overcome these limitations, such as the use of natural compounds, either alone or in combination with conventional chemotherapeutic agents. In the present study, curcumin (CUR), a polyphenolic compound with promising anticancer properties, was combined with cisplatin (CIS), a widely used chemotherapeutic agent, to evaluate their *in vitro* effects on the A375 melanoma cell line. The cytotoxicity assessment was based on the MTT method, followed by investigations of the impact on mitochondrial function using the JC-1 assay and MitoTracker staining. Additionally, the impact on nuclei, actin filaments, and tubulin was analyzed using immunofluorescence techniques, as well as the proapoptotic and necrotic potential of the tested compounds. The results showed a predominantly additive effect, with synergy emerging at the highest tested concentration relative to the individual treatments.

Rezumat

Melanomul este una dintre cele mai agresive și letale forme de cancer cutanat, iar în pofida progreselor terapeutice recente, eficacitatea tratamentului este adesea limitată de rezistența la medicamente și de profilurile de siguranță nesatisfăcătoare. Prin urmare, o atenție tot mai mare a fost îndreptată către abordări alternative capabile să depășească aceste limitări, precum utilizarea compușilor naturali, fie singuri, fie în combinație cu agenți chimioterapeutici convenționali. În studiul de față, curcumina (CUR), un compus polifenolic cu proprietăți anticanceroase promițătoare, a fost combinată cu cisplatina (CIS), un agent chimioterapeutic utilizat pe scară largă, pentru a evalua efectele lor *in vitro* asupra liniei celulare de melanom A375. Evaluarea citotoxicității s-a bazat pe aplicarea metodei MTT, urmată de investigații privind impactul asupra funcției mitocondriale, prin intermediul testului JC-1 și al colorării cu MitoTracker. Adițional, a fost analizat impactul asupra nucleilor, filamentelor de actină și tubulină prin aplicarea tehnicilor de imunofluorescență, precum și potențialul proapoptotic și necrotic al compușilor testați. Rezultatele au indicat un efect predominant aditiv, observându-se o sinergie la cea mai mare concentrație testată, în comparație cu tratamentele individuale.

Keywords: melanoma, cisplatin, curcumin, cytotoxicity, combined treatment

Introduction

Globally, skin cancer is one of the most frequently occurring types of cancer, with approximately 3.3 million new cases diagnosed every year and a constantly increasing incidence, due to numerous factors (1). Overexposure to ultraviolet (UV) radiation is still the most important risk factor, but environmental conditions, such as higher levels of air pollution, can also play a critical role. Moreover, lifestyle factors, such as poor dietary habits, combined with genetic predisposition and immunosuppression, may further increase the risk of developing skin cancer (2). From a clinical perspective, skin cancers are classified into two major categories. First, there is non-melanoma skin cancer (NMSC), the most often diagnosed type, which consists of basal cell

carcinoma (BCC) and squamous cell carcinoma (SCC) (3). These forms typically have a slower progression and a lower risk of metastasis. Second is melanoma, a less prevalent but more aggressive form of cancer recognized for its rapid progression, higher metastatic potential, and major contribution to skin cancer-related deaths (4). Nonetheless, some of the distinctive properties of melanoma, such as its high capacity for migration and increased invasive potential, can be viewed in light of the origin of melanocytes (specialized cells that produce the pigment melanin).

Malignant melanoma is a disease arising from the neural crest, an embryonic formation whose cells have an intrinsic capacity to migrate and colonize multiple target tissues during development. As melanocyte precursors, neural crest-derived cells influence melanocyte behavior throughout their lifetime, retain their migratory properties, and promote the invasive phenotype associated with melanoma (5). Currently, although there have been advances in standard cancer treatments such as radiation therapy and chemotherapy, together with modern immunotherapy and targeted therapies, there are still significant challenges related to drug resistance and treatment-associated toxicity, including low bioavailability, possibly serious side effects, or an unfavorable pharmacological response (6, 7).

In this regard, current research is focusing on discovering new therapeutic agents, with plant-based compounds proving to be valuable candidates because of their demonstrated anti-cancer properties and, in general, an acceptable safety profile (8). Furthermore, natural compounds with pro-apoptotic, antiproliferative, and antioxidant properties have shown promising potential as complementary or standalone treatments for various skin malignancies, as they target molecules and signaling pathways that play key roles in cancer initiation, such as by interfering with angiogenesis and enhancing caspase activity (9). At the same time, the combination of phytocompounds with classical chemotherapeutic agents that are therapeutically ineffective or have an unfavorable safety profile has increasingly attracted researchers' attention in the field (10).

One of these plant-derived compounds is curcumin (CUR), a phytochemical from *Curcuma longa*, a member of the polyphenol class. It is widely used in Asian countries in traditional medicine, mainly for its therapeutic properties, including antioxidant and anti-inflammatory effects and pain-relieving benefits (11). Nevertheless, it continues to attract attention in modern medicine due to its proven benefits in the management of certain chronic diseases, such as Alzheimer's and cardiovascular disease, while also standing out for its potential in treating certain types of cancer. This effect appears to be attributed to CUR's ability to regulate certain key molecules involved in cancer progression, such as CDK2, CK2α, EGFR, NF-κB, and the AXL tyrosine kinase receptor (12).

Cisplatin (CIS) is a drug used to treat melanoma, cancers of the genitourinary system, head and neck cancers, and lung cancer. The anticancer activity of CIS is primarily due to DNA damage and the activation of pro-apoptotic pathways. However, its side effects and resistance limit its use and efficacy (13). CIS was selected as the reference cytotoxic agent because it is used in several melanoma treatment protocols but its efficacy is limited by the intrinsic chemoresistance of this tumor and by dose-dependent toxicity (14). The association with a chemosensitizing compound such as CUR is the hypothesis of the present study, which posits that it could potentiate the cytotoxic effect at lower concentrations (15). In this context, the present study aimed to evaluate the cytotoxic effects of CIS, CUR, and their combination on melanoma using the A375 cell line. Specifically, the study investigated their effects on cell viability and morphology, as well as their impact on mitochondrial function. Furthermore, the effects of the treatments on nuclei, actin filaments, and tubulin organization were evaluated, together with their potential to induce apoptosis and necrosis.

Materials and Methods

Specific reagents and instruments

CUR, CIS, phosphate-buffered saline (PBS), Acridine Orange, Propidium Iodide, and Triton X-100 were purchased from Sigma-Aldrich (Merck KGaA, Darmstadt, Germany). Trypsin-EDTA solution, fetal bovine serum (FBS), penicillin/streptomycin solution (100 U/mL–100 μg/mL), and Dulbecco's Modified Eagle's Medium (DMEM) were obtained from PAN-Biotech GmbH (Aidenbach, Germany). The MTT assay kit (3-(4,5-dimethylthiazol-2-yl)-2,5-diphenyltetrazolium bromide) was obtained from Roche (United Kingdom). Hoechst 33342 stain, MitoTracker™ Red CMXRos, Texas Red™-X phalloidin dye, alpha-tubulin mono-clonal antibody (B-5-1-2), and goat anti-mouse IgG (H+L) secondary antibody (Alexa Fluor™ 488) were purchased from Thermo Fisher Scientific (Waltham, MA, USA). The JC-1 Mitochondrial Membrane Poten-tial Assay Kit was purchased from Elabscience (Houston, TX, USA). The 4% paraformaldehyde in PBS was obtained from Santa Cruz Biotechnology (Dallas, TX, USA). Bovine serum albumin (BSA) was purchased from Cell Signaling Technology (Danvers, MA, USA). The Cytation 5 multimode plate reader, Lionheart FX automated microscope, and Gen5™ Microplate Data Collection and Analysis Software (Version 3.14) were provided by BioTek Instruments (Winooski, VT, USA).

Cell line and culture conditions

A375 (CRL-1619™) cell line, derived from a 54-year-old female with malignant melanoma, was cultured in a specific growth medium, Dulbecco's Modified Eagle's Medium (DMEM) supplemented with 10% fetal bovine serum and 1% antibiotics. The CIS stock solution was 5 mM (dissolved in ultrapure water), while the CUR stock solution was 5 mM (dissolved in DMSO, maximum concentration did not exceed 0.5%). Dilutions were prepared from the stock solutions in the culture medium. CIS was tested at concentrations of 1, 2, 3, 4, and 5 μM, while CUR was evaluated at 1, 5, 10, 20, and 30 μM. In addition, combinations of the two compounds were prepared as follows: CIS 1 μM + CUR 1 μM; CIS 2 μM + CUR 5 μM; CIS 3 μM + CUR 10 μM; CIS 4 μM + CUR 20 μM; and CIS 5 μM + CUR 30 μM.

Cell Viability evaluation using MTT assay

The first step in assessing cytotoxicity was to determine cell viability using the MTT assay. A375 cells were seeded in 96-well plates at a density of 1×10^4 cells/well, and after achieving a confluence of approximately 70%, they were exposed for 24 hours to CIS at concentrations of 1, 2, 3, 4, and 5 μM, to CUR at concentrations of 1, 5, 10, 20, and 30 μM, along with combinations of the two agents (CIS 1 μM + CUR 1 μM; CIS 2 μM + CUR 5 μM; CIS 3 μM + CUR 10 μM; CIS 4 μM + CUR 20 μM; and CIS 5 μM + CUR 30 μM). Upon ending the treatment period, the culture medium was replaced with fresh medium, and 10 μL/well of MTT solution was added. The plates were then incubated for 3 hours at 37°C in a humidified atmosphere containing 5% CO_2. Then, 100 μL/well of MTT solubilization solution was added, and the plates were incubated at room temperature in the dark for 30 minutes. Lastly, absorbance was measured at 570 and 630 nm using the Cytation 5 microplate reader (BioTek Inc., USA).

Drug interaction analysis

To evaluate the pharmacological interaction between CIS and CUR, a median-effect analysis was performed using the Chou-Talalay method. Quantitative parameters, including the fraction affected (Fa), the dose-reduction index (DRI), and the combination index (CI), were calculated utilizing CompuSyn software (version 1.0; CompuSyn, Inc., Paramus, NJ, USA). The nature of the drug interaction was categorized based on CI values, where CI < 1 indicates synergism, CI = 1 denotes an additive effect, and CI > 1 represents antagonism. Furthermore, a DRI value greater than 1 (DRI > 1) signifies a favorable dose-reduction capacity, indicating that the therapeutic combination allows for a concentration decrease of the individual compounds relative to their respective monotherapies (16).

Cell morphology evaluation using Bright field microscopy

To evaluate the effect of the treatment on A375 cells, bright-field microscopy was performed. The cells were cultured in 96-well plates and, after reaching adequate confluence, were treated for 24 hours with CIS, CUR, and their combinations at the concentrations mentioned above. Representative images were taken at the end of the treatment period using the Lionheart FX automated microscope.

Mitochondrial membrane potential (ΔΨm) assay – JC-1 staining

To examine the effects of CIS, CUR, and their combination on the mitochondrial membrane potential (ΔΨm) of A375 cells, a JC-1-based mitochondrial membrane potential assay was used, following the method described by Talpos *et al*. (17). Briefly, A375 cells were seeded at a density of 1×10^4 cells/well in black-walled, clear-bottom 96-well plates. When confluence was approximately 70%, the cells were treated for 24 hours with CIS (5 μM), CUR (30 μM), and a combination of the two compounds (CIS 5 μM + CUR 30 μM). The culture medium was discarded at the end of the treatment period, followed by gentle washing of the cells with PBS. Afterward, the cells were incubated with JC-1 dye (5 μM, 100 μL/well) for 45 minutes at 37°C, then washed twice with PBS to remove residual dye, and fluorescence images were obtained using a Lionheart FX automated microscope. The red and green fluorescence intensities were quantified at 590 nm and 529 nm, respectively, using a Cytation 5 multimodal reader.

Mitochondrial assessment using MitoTracker™ red CMXRos

For the purpose of assessing the effect of the treatment on mitochondria, A375 cells were seeded into 12-well plates at a density of 1×10^5 cells *per* well. Upon reaching proper confluence, cells were treated for 24 hours with CIS at a concentration of 5 μM, CUR at a concentration of 30 μM, and a combination of the two compounds (CIS 5 μM + CUR 30 μM). After the treatment period, the cells were incubated for 30 minutes in a MitoTracker Red CMXRos solution diluted in the culture medium to a final concentration of 300 nM from a 1 mM stock prepared in DMSO. Following the incubation period, the cells were washed twice with PBS to remove excess reagents. Representative fluorescent images were subsequently acquired using the Lionheart FX Automated Microscope. A similar protocol was previously described by Dan *et al*. (18).

Immunofluorescence staining of nuclei, tubulin, and F-actin filaments

The impact of the 24 hours of treatment with CIS at a concentration of 5 μM, CUR at a concentration of 30 μM, and the combination of the two compounds (CIS 5 μM + CUR 30 μM) on nuclear morphology

and the distribution of cytoskeletal F-actin and tubulin filaments was investigated by immunofluorescence staining. Initially, A375 cells were seeded at a density of 1×10^4 cells/well in clear-bottom, black 96-well plates and allowed to attach. After reaching the appropriate confluence, the cells were exposed to CIS, CUR, and their combination at the previously mentioned concentrations. Post-treatment, cells were fixed with 4% paraformaldehyde for 15 minutes, then washed twice with PBS. Next, cells were permeabilized with 50 µL/well of 0.1% Triton X-100 and incubated at room temperature for 15 minutes, and then washed twice with PBS. Then, the cells were blocked with 100 µL/well of 1% bovine serum albumin (BSA) and kept at room temperature for 30 minutes. Tubulin was stained by incubating the cells with 50 µL/well of anti-α-tubulin monoclonal antibody (B-5-1-2) diluted 1:500 in 1% BSA for 3 hours, with subsequent 45-minute incubation with a secondary goat anti-mouse IgG (H+L) antibody conjugated to Alexa Fluor™ 488, diluted 1:500. After washing the cells two times with PBS, a staining mix containing phalloidin Texas Red™-X diluted 1:200 for F-actin visualization and Hoechst 33342 diluted 1:2000 for nuclear staining (50 µL/well) was applied. The cells were incubated for 30 min at room temperature in the dark. Finally, the cells were washed twice with PBS, and fluorescent images were acquired using the Lionheart FX Automated Microscope and analyzed using the Gen5™ Microplate Data Collection and Analysis Software Version 3.14 (BioTek Inc., USA). A similar protocol was previously described by Marcovici *et al*. (19).

Acridine Orange/Propidium Iodide (AO/PI) Assay

The effects of CIS, CUR, and their combination on the viability of A375 cells and membrane integrity were assessed using a dual-staining assay with acridine orange/propidium iodide (AO/PI). A375 cells were seeded in 96-well plates at a density of 1×10^4 cells/well and exposed for 24 hours to CIS (5 µM), CUR (30 µM), or the combination treatment (CIS 5 µM + CUR 30 µM). After exposure, 100 µL of AO/PI staining solution prepared in complete culture medium (Acridine Orange, 10 µg/mL; propidium iodide, 10 µg/mL) was added to each well. The plates were then incubated for 10 minutes at room temperature, protected from light, after which fluorescence images were acquired using a Lionheart FX automated microscope (20).

Statistical analysis

The data obtained from the statistical analysis were presented as mean ± standard deviation (SD). The normality of the data distribution was tested using the Shapiro–Wilk test. Given that the data set had a normal distribution, a one-way ANOVA was performed for statistical analysis, which was followed by the Dunnett test for multiple comparisons as a post hoc analysis. Statistical analyses were performed using GraphPad Prism software, version 10.2.3 (GraphPad Software, San Diego, California, USA). The threshold for statistical significance was set at $*p < 0.05$, and higher levels of significance were denoted as follows: $**p < 0.01$, $***p < 0.001$, and $****p < 0.0001$. The experiments were conducted in three independent biological replicates, each containing three technical replicates.

Results and Discussion

The concentrations of CIS and CUR were selected based on literature data to cover a wider range and demonstrate their biological effects (21-24). As for CIS concentrations (1-5 µM), they were chosen to be near the free, pharmacologically active fraction observed in patients' plasma, where the maximum concentration of free platinum is around 5-6 µM. In this way, testing at supraclinical levels that could induce non-specific cytotoxic effects is avoided (25, 26). For CUR, the wider range tested (1 - 30 µM) is due, firstly, to its low oral bioavailability and, secondly, to the modest plasma concentrations reported. The concentration range for CUR was chosen to fully cover the dose–response curve, intentionally exceeding the nanomolar plasma concentrations achieved following oral administration. Therefore, the tested micromolar concentrations should be regarded primarily as exploratory and mechanistic *in vitro* conditions, while formulations with improved bioavailability remain an area of ongoing investigation (27, 28).

Combined cytotoxic activity of CIS and CUR treatment in A375 cells

The first phase in assessing the cytotoxic potential of CIS, CUR, and their combination was to determine A375 cell viability using the MTT assay 24 hours after treatment (Figure 1). Upon treatment with CIS, a dose-dependent decrease in A375 cell viability was observed. Cell viability decreased from 96.16% at 1 µM to 84.36%, 78.57%, 72.88%, and 44.79% at concentrations of 2, 3, 4, and 5 µM, respectively. Likewise, treatment with CUR induced a progressive reduction in cell viability, with values of 86.18%, 79.33%, 72.83%, 61.77%, and 53.80% at concentrations of 1, 5, 10, 20, and 30 µM, respectively. A more pronounced cytotoxic effect was observed with the combination treatment compared with the individual treatments. After combined treatment with CIS and CUR (CIS 1 µM + CUR 1 µM; CIS 2 µM + CUR 5 µM; CIS 3 µM + CUR 10 µM; CIS 4 µM + CUR 20 µM; CIS 5 µM + CUR 30 µM), the viability of A375 cells was 82.65%, 67.74%, 54.29%, 47.13%, and 26.57%, respectively.

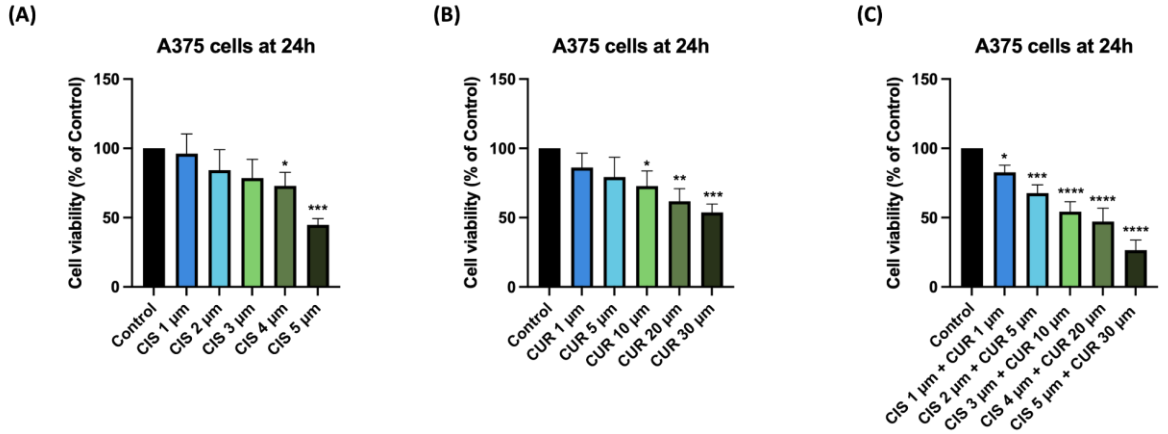

Figure 1.

Graphical representations of the effect induced by A) CIS, B) CUR, and C) CIS + CUR on A375 cell viability after 24 hours of treatment. The results are expressed as percentages (%) normalized to the untreated control group. Data are presented as mean values ± standard deviation (SD) from three independent experiments, each performed in triplicate. Statistical differences between the treated groups and the control were assessed using one-way ANOVA followed by Dunnett's multiple comparisons post hoc test (*p < 0.05; **p < 0.01; *** p <0.001; **** p < 0.0001).

To determine cell viability, the MTT assay was used, a standard colorimetric method that quantifies metabolically active cells by measuring the activity of mitochondrial reductases that convert tetrazolium salts to formazan. The selection of this method was based on its reproducibility, simplicity, and extensive use in cytotoxicity studies on the A375 cell line, which facilitates direct comparison of the results with existing data in the literature (29, 30). Viability assessment was performed at the 24-hour time point to capture early cytotoxic effects and minimize interference from secondary processes, cell repopulation, nutrient depletion from the medium, and instability of CUR in the culture medium, that may distort interpretation at longer time points (31). This time point also allows attribution of the observed effect to the direct action of the compounds rather than to late mechanisms, such as prolonged cell-cycle arrest. Furthermore, previous *in vitro* studies in A375 cells used the 24-hour time point, which facilitates comparability (30). Similar studies have indicated a variable IC_{50} for CUR, dependent on the testing time. Thus, in the study by Zhao and collaborators, CUR exhibited an IC_{50} of 25 µM at the 24-hour testing interval (29). Other studies have indicated an increase in IC_{50} up to 80 µM at the 48-hour testing interval (32). In the case of CIS, previous studies support the relative chemoresistance of melanoma to this classic chemotherapy. The IC_{50} values previously tested for this chemotherapy showed large variations, depending on cell density and exposure duration (33, 34). The stronger association between CUR and CIS suggests a potential synergistic interaction, consistent with observations that CUR sensitizes tumor cells to CIS (15, 35).

The nature of the interaction between CIS and CUR was further evaluated using the Chou-Talalay method. The CI values varied according to the effect level (Table 1). At low and intermediate concentrations, the CI values were close to unity (0.858-0.971), indicating a predominantly additive effect. In contrast, at the highest combination tested (CIS 5 µM + CUR 30 µM), a CI of 0.602 was obtained, indicating a synergistic interaction. The dose-reduction index (DRI) was greater than 1 for both agents at all tested levels, indicating that the combined cytotoxic effect can be achieved using lower doses of each compound than would be required in monotherapy.

Table I

Combination index (CI) and dose-reduction index (DRI) values for the CIS + CUR association in A375 cells, calculated according to the Chou-Talalay method

Combination	Fa	CI	DRI (CIS)	DRI (CUR)	Interpretation
CIS 1 µM + CUR 1 µM	0.173	0.858	2.39	2.28	Slight synergism
CIS 2 µM + CUR 5 µM	0.323	0.951	1.84	2.45	Additive
CIS 3 µM + CUR 10 µM	0.457	0.855	1.66	3.96	Slight synergism
CIS 4 µM + CUR 20 µM	0.529	0.971	1.45	3.57	Additive
CIS 5 µM + CUR 30 µM	0.734	0.602	1.86	15.20	Synergism

Fa - fraction affected; CI - combination index (CI < 1 synergism, CI = 1 additivity, CI > 1 antagonism); DRI - dose-reduction index. Values were calculated from mean viability data obtained by the MTT assay

Combined CIS and CUR treatment induces significant morphological changes in A375 cells

In the next step of evaluating the cytotoxicity of the 24-hour treatment with CIS, CUR, and their combination, the impact on cell morphology was assessed (Figure 2). Thus, in the case of CIS treatment, starting at a concentration of 2 μM, a slight decrease in confluence was observed, along with changes such as cell shrinkage or rounding; depending on the administered dose, the most significant changes occurred at the highest concentration (5 μM). In the case of CUR treatment, a dose-dependent decrease in confluence was observed, along with morphological changes starting at 10 μM, including cell rounding, and at the highest administered concentration, cell blebbing was also observed. However, in the case of the combined treatment, all the morphological changes mentioned and the decrease in confluence were more pronounced, accompanied by marked cell fragmentation, particularly with CIS 5 μM + CUR 30 μM.

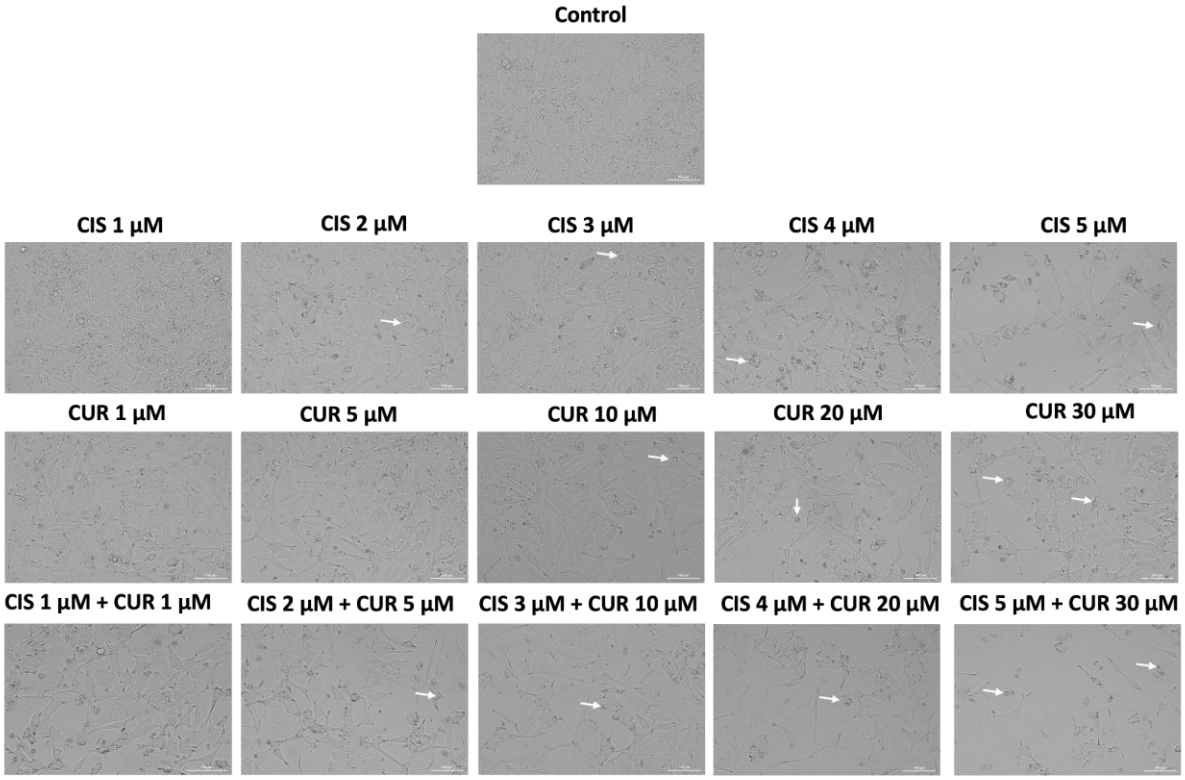

Figure 2.

Morphological and confluence changes in A375 cells (white arrows) following 24 hours of treatment with CIS, CUR, and combinations of the two compounds. The scale bar indicates 100 μm.

Morphological evaluation of cells is an important step in assessing compound cytotoxicity, as phase-contrast optical microscopy allows identification of the main types of cell death based on characteristic structural changes. The A375 cell line is characterized by an adherent, fusiform/epithelioid morphology and growth in a confluent monolayer. Changes in these characteristics, such as loss of intercellular contacts, rounding, or detachment from the substrate, are clear indicators of cellular damage. Recent data from the melanoma literature indicate that tumor cells lose their characteristic morphology in response to treatment, whereas normal melanocytes are unaffected. Thus, a study conducted on G361 melanoma cells indicated cellular morphological changes such as size reduction, membrane blebbing, and decreased cell density, all of which indicate signs of cell death (36).

Regarding the mechanism of cell death, the morphological changes associated with apoptosis and necrosis are different. Apoptosis is characterized by a sequence of events such as: cell shrinkage, membrane blebbing, chromatin cleavage, nuclear condensation, and the formation of pyknotic bodies of condensed chromatin. As the process progresses, cells undergo a size reduction, lose contact with neighboring cells and the extracellular matrix, and, upon detachment, adopt a rounded morphology; subsequently, blebs separate, forming dense apoptotic bodies packed with organelles and nuclear fragments (37, 38). On the other hand, necrosis is characterized by swelling of the cytoplasm and cytoplasmic organelles, and rupture of the plasma membrane. An additional

criterion for differentiation is the kinetics of these processes: stimuli that initiate apoptosis usually require 8–20 hours to cause these changes, while necrotic stimuli often produce morphological alterations within 2–3 hours (39). The fact that the changes were observed at 24 hours of treatment is therefore compatible with an apoptotic-type process.

The results of the present study describe morphological changes characteristic of apoptosis, which manifest in a dose-dependent manner. The cell rounding and shrinkage observed in the case of treatment with CIS, starting from the concentration of 2 μM, and with CUR, starting from 10 μM, correspond to the early stages of apoptosis, characterized by loss of adhesion and cell retraction. The membrane blebbing highlighted at the maximum concentration of CUR (30 μM) represents one of the hallmarks of apoptosis, and the marked cell fragmentation, observed especially in the case of the combined treatment CIS 5 μM + CUR 30 μM, corresponds to the advanced stage of the process, namely the formation of apoptotic bodies by the separation of blebs. The dose-dependent nature of these changes, as well as their intensification under the combined treatment, is consistent with the results obtained by the MTT viability test and with the values of the CI, providing an independent morphological corroboration of the quantified cytotoxic effect.

Literature data support the results obtained. CUR has been previously studied in the melanoma cell line SK-Mel-37, which showed morphological changes such as plasma membrane blebbing, apoptotic body formation, chromatin condensation, and nuclear segregation in cells treated with 10–20 μM, a range that overlaps with the observations in the present study (40). Similarly, a study conducted on melanoma cells indicated the presence of cellular changes - cell shrinkage, membrane blebbing, and decreased cell density after exposure to CUR (36). As for CIS, it is well documented that it exerts various effects on tumor cell morphology, including cell shrinkage, nuclear alterations, cytoplasmic blebbing, apoptotic body formation, loss of cell adhesion, and membrane blebbing alterations, which is considered one of the hallmarks of CIS-induced apoptosis (41). The previous study on the association of CIS with CUR indicated that both the individual compounds and their combination induce changes similar to those observed in the present study (42). Thus, the present data are consistent with data obtained and previously discussed in the literature.

Combined CIS and CUR treatment induced loss of mitochondrial membrane potential in A375 cells

Based on the results of the MTT assay, the cytotoxicity assessment was continued by determining the treatment's impact on mitochondrial function, specifically on mitochondrial membrane potential, using the JC-1 assay. Microscopic images (Figure 3A) showed a reduction in mitochondrial membrane potential relative to the control, marked by a predominance of green fluorescence (JC-1 monomers) over red fluorescence (JC-1 aggregates) in all treatment groups. However, the most pronounced effect was observed with the combined treatment, indicating the greatest depolarization of the mitochondrial membrane potential. These results were also confirmed by quantitative analysis (Figure 3B), where the results were expressed as the JC-1 aggregate/monomer ratio. In this case, the results were as follows: for CIS at 5 μM: 46%, for CUR at a concentration of 30 μM: 57.19%, and for the combined treatment with CIS 5 μM + CUR 30 μM, the value was 16.83%.

Mitochondrial membrane potential (Δψm) analysis is a crucial step for assessing mitochondrial function in cytotoxicity studies. This parameter reflects mitochondria's ability to produce energy via oxidative phosphorylation and is a key marker of cellular metabolic status. Changes in ΔΨm can indicate enhanced cellular stress and are frequently associated with incipient pro-apoptotic alterations. Depolarization of the mitochondrial membrane is linked to apoptotic cell death, as it increases mitochondrial membrane permeability, leading to the cytosolic release of cytochrome c. This triggers the mitochondrial apoptotic pathway, with caspases and other pro-apoptotic proteins, especially caspases 3/7, 8, and 9, getting activated (43). The JC-1 test is based on the ability of this cationic dye to accumulate in mitochondria, a process that depends on the mitochondrial membrane potential. Normally, in healthy cells with polarized mitochondria, the dye forms JC-1 aggregates that emit red fluorescence. Alternatively, under cellular stress, if the mitochondrial membrane potential is depolarized, the dye remains monomeric, producing green fluorescence. Therefore, the ratio between red (aggregates) and green (monomers) fluorescence serves as a sensitive indicator of mitochondrial functional status (44). This study reports that the decrease in the JC-1/monomer ratio observed in all treated groups, particularly after combination therapy, relative to the control group, along with the dominance of green fluorescence following treatment, suggests that the treatment may induce mitochondrial membrane depolarization, thereby potentially triggering the mitochondrial apoptotic pathway. Similar findings have been described in pancreatic cancer cell lines, such as MIA PaCa-2 and PANC-1, where CIS and CUR, administered individually and in combination at concentrations of 5, 15, and 25 μM, caused mitochondrial membrane depolarization, based on the reduction in JC-1 aggregate/monomer ratio, suggesting significant mitochondrial dysfunction and early apoptosis (45). In other pancreatic cancer cell lines, such as BxPC-3 and YAPC, treatment with CIS alone has

been found to induce a time-dependent loss of mitochondrial membrane potential, indicating the onset of early apoptotic changes (22). In addition, Kocyigit *et al*. found that CUR, at concentrations ranging from 5 to 50 µM, decreased mitochondrial membrane potential after 24 hours of treatment in the murine melanoma cell line B16F10 (46). Also, Qiu and colleagues examined the effect of CUR at concentrations up to 50 µg/mL on the WM-115 melanoma cell line after 6 hours of treatment, and the results showed a reduction in mitochondrial membrane potential (47).

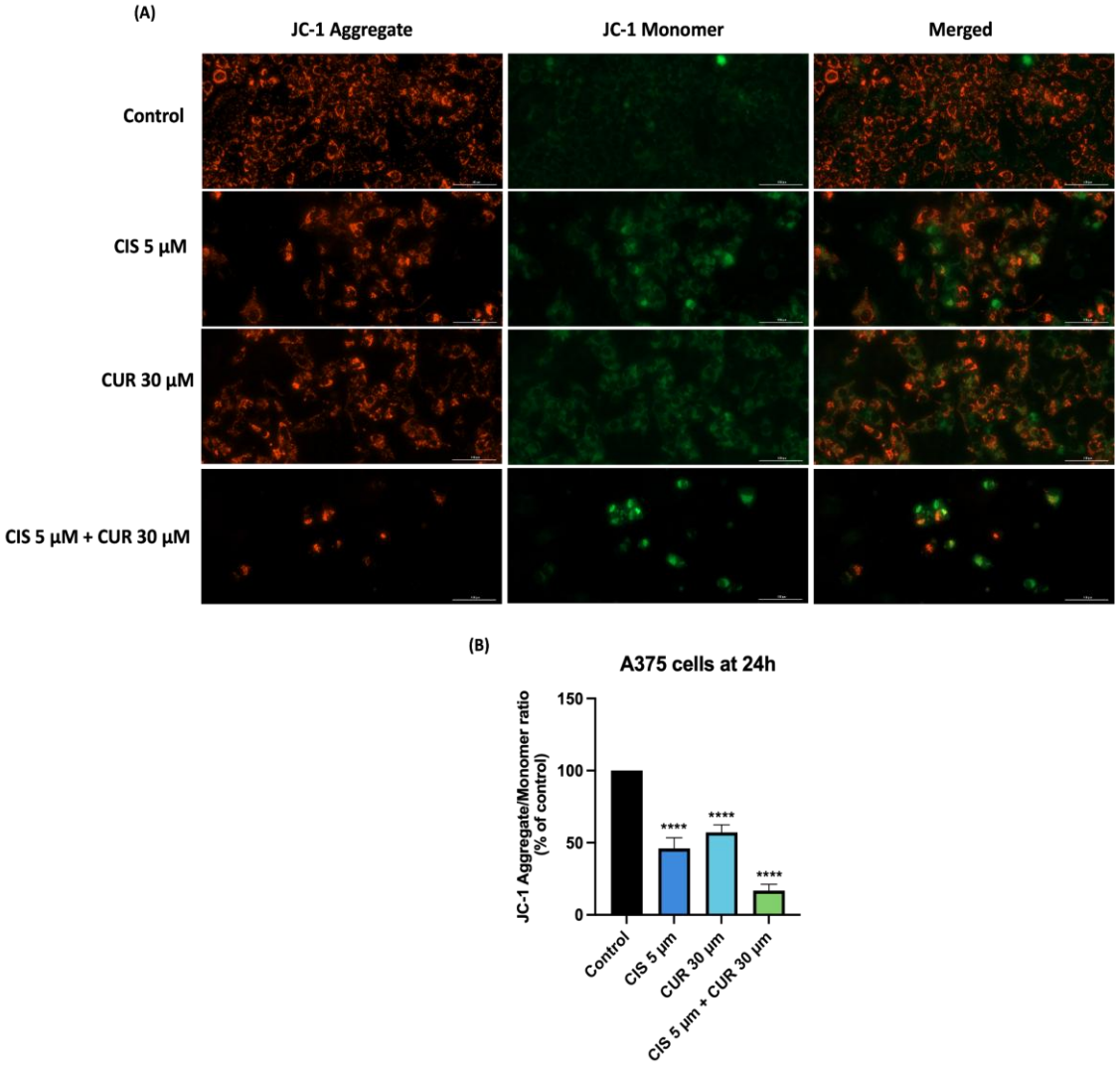

Figure 3.

The effect of treatment on mitochondrial membrane potential of A375 cells following 24 hours of treatment with CIS, CUR, and a combination of the two compounds. A) Representative images of the JC-1 assay, where red indicates JC-1 aggregates and green indicates JC-1 monomers. B) A graphical representation showing the JC-1 aggregate/monomer ratio. Data are presented as mean values ± SD from three independent experiments, each performed in triplicate. Statistical differences between the treated groups and the control were assessed using one-way ANOVA followed by Dunnett's post hoc test for multiple comparisons (**** $p < 0.0001$)

Combined CIS and CUR treatment induces mitochondrial alterations in A375 cells

Following the observed loss of mitochondrial membrane potential induced by CIS, CUR, and especially their combined treatment, mitochondrial morphology staining was further performed to evaluate the associated mitochondrial damage. Microscopic analysis of mitochondrial morphology in A375 cells (Figure 4) treated with CIS (5 µM), CUR (30 µM), and the combination of CIS 5 µM + CUR 30 µM revealed marked structural alterations, characterized by mitochondrial fragmentation with the appearance of condensed, punctate mitochondria, reduced in number compared to the control, along with focal areas of increased fluorescence intensity reflecting mitochondrial clustering. These changes were most pronounced with the combined treatment.

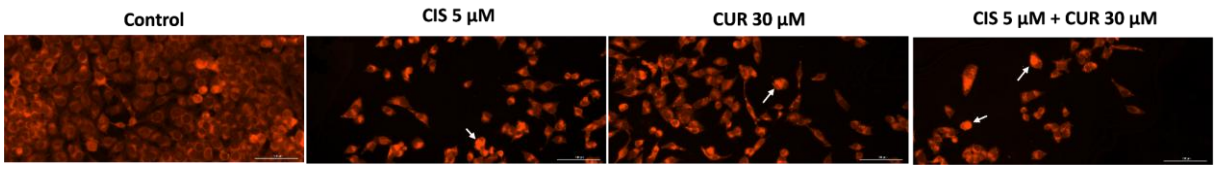

Figure 4.
Representative images of the impact of CIS, CUR, and combinations of the two compound treatments (24 hours) on mitochondria morphology in A375 cells. The white arrows show mitochondrial changes. The scale bar was 100 µm

MitoTracker dyes are commonly used to assess mitochondrial morphology because they selectively accumulate in active mitochondria, enabling clear visualization of mitochondrial structure and integrity (48).

The evaluation of mitochondrial morphology is an important step in elucidating potential biological mechanisms underlying cell death, as mitochondria are central to the regulation of apoptosis (49). Mitochondrial fragmentation, manifested by the appearance of condensed, punctate mitochondria and a reduction in their number compared to the control, represents a morphological change characteristic of apoptosis. Mitochondria are dynamic organelles whose morphology is regulated by the balance between fusion and fission; during apoptosis, this balance is disrupted in favor of fission (50, 51). Thus, during apoptosis, mitochondria undergo extensive fragmentation that precedes caspase activation, resulting in a smaller, more numerous mitochondrial network (52). Studies in the field have indicated that elongated mitochondria confer resistance to apoptosis in cells, while fragmented mitochondria increase cellular sensitivity to apoptotic stimuli (53). Therefore, the mitochondrial fragmentation observed in the present study, which was most pronounced with the combined treatment, is consistent with the apoptotic profile indicated by the other results.

An important aspect to note is the concordance between the decrease in membrane potential as indicated by JC-1 and the morphological fragmentation visualized by MitoTracker Red CMXRos staining. The results obtained lead to the same conclusion: a pronounced mitochondrial dysfunction is involved, amplified by the association of the two compounds. MitoTracker Red CMXRos is a fluorescent dye that accumulates in mitochondria; its accumulation depends on the membrane potential, which is why it is frequently used to visualize mitochondrial structure and integrity (54). The focal increase in fluorescence intensity observed in areas with condensed mitochondria most likely reflects the aggregation and clustering of fragmented organelles, rather than increased mitochondrial activity. This interpretation is consistent with the loss of membrane potential demonstrated by JC-1 and is supported by the observation that, in the case of CMXRos, the fluorescence intensity does not exclusively reflect the mitochondrial potential, as the dye covalently binds to thiol groups in mitochondrial lipids and proteins.

These results indicate the possible involvement of the intrinsic apoptotic pathway in the death of A375 melanoma cells induced by CIS and CUR, with the association of the two compounds producing the most pronounced mitochondrial dysfunction.

Combined CIS and CUR treatment induces significant alterations in nuclei, actin filaments, and tubulin organization in A375 cells

The investigation continued by assessing the impact on specific cellular components, including nuclei, actin filaments, and tubulin (Figure 5). Following treatment with 5 µM CIS, 30 µM CUR, and 5 µM CIS + 30 µM CUR, chromatin condensation and nuclear rounding were observed; the effects were more pronounced with the combined treatment. Moreover, a significant increase in the apoptotic index compared to the control was obtained: 15.29% for CIS, 12.02% for CUR, and 28.33% for the combined treatment.

In the case of actin filaments, disorganization of the filament network and cell shrinkage were observed, with the most pronounced effect seen in the combination treatment. Similarly, the tubulin network displayed disorganization, accompanied by cell rounding. For both actin and tubulin, the most pronounced morphological alterations were observed in the combination treatment (Figure 5).

Because changes in the nucleus, actin filaments, and tubulin can provide additional information about the mechanism of cell death, the next step was to investigate the effects of CIS, CUR, and the combination at this level (55). Chromatin condensation and nuclear rounding are specific changes of cell apoptosis. In addition, nuclear fragmentation is a defining characteristic of apoptotic death and is one of the classical morphological criteria used to identify apoptotic cells (56). Unlike the general morphological assessment, quantification of the apoptotic index provides an objective, semiquantitative measure of apoptosis induction, which strengthens the interpretative value of the results.

Importantly, the apoptotic index of the combination (28.33%) is approximately equal to the sum of the individual effects of the two agents (15.29% +

12.02% = 27.31%), suggesting a predominantly additive effect on apoptosis induction. This observation is consistent with the results of the Chou-Talalay analysis, in which most combinations showed an additive character, as well as with the results of the viability test, thus providing internal coherence to the set of experimental data.

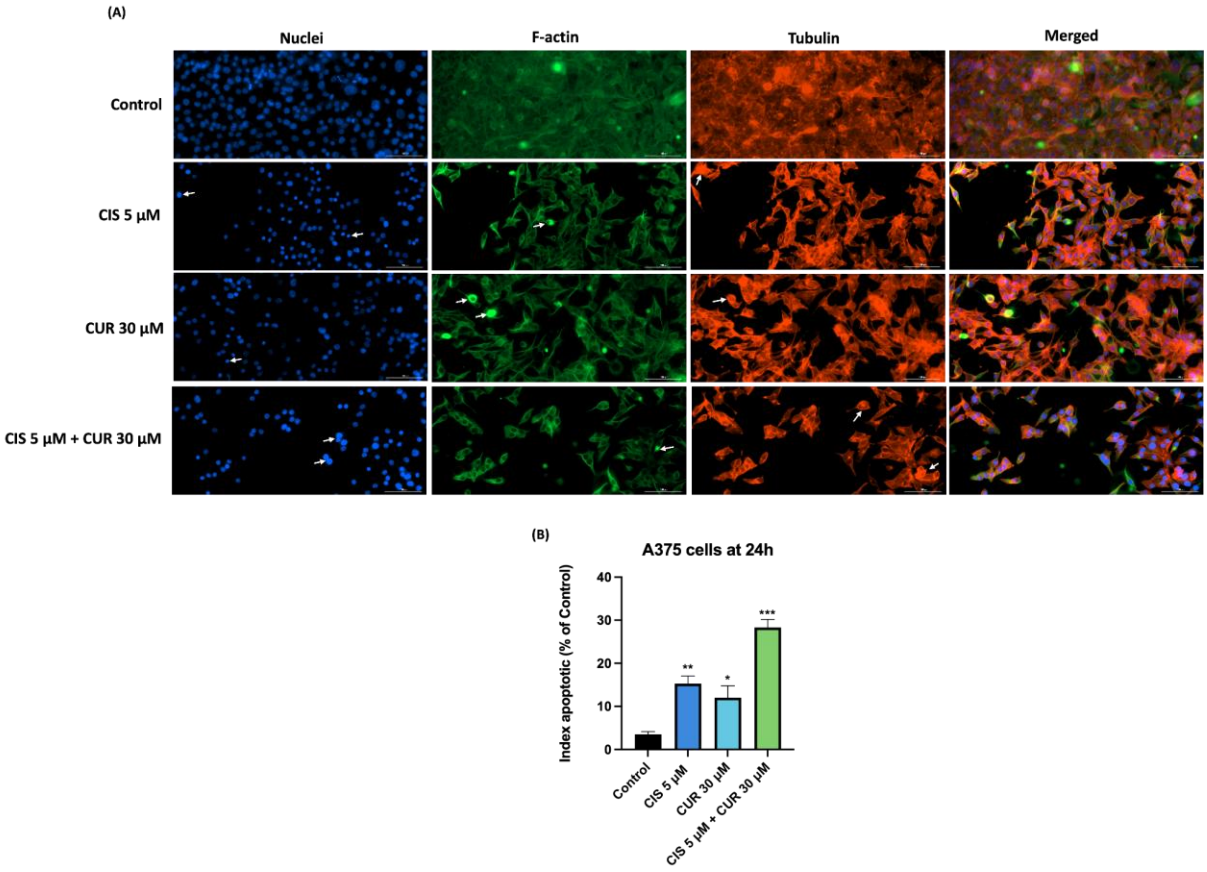

Figure 5.

The effect of treatment with CIS, CUR, and their combination on A375 cells, as shown by nuclear, F-actin, and tubulin staining after 24 hours of treatment. A) Representative microscopic images of cellular components. B) Graphical representation of the apoptotic index. Data are presented as mean values ± SD from three independent experiments, each performed in triplicate. Statistical differences between the treated groups and the control were assessed using one-way ANOVA followed by Dunnett's multiple comparisons post hoc test (*p < 0.05; **p < 0.01; *** p <0.001)

In addition to the nuclear-level changes, the tested compounds induced cytoskeletal disorganization, visible both in actin filaments and in the tubulin network. Actin filament reorganization is closely linked to apoptotic morphological changes, since cell rounding, blebbing, and the formation of apoptotic bodies are consequences of actin reorganization, and actin dynamics can activate and mediate apoptosis (57). Previous studies have evaluated the impact of CUR on actin filament and tubulin levels. In the study by Zhou and collaborators, it was reported that CUR induces apoptosis in A549 cells and causes disorganization of the actin cytoskeleton, which supports the alterations in actin filaments observed in our study (58). It has also been documented that CUR directly interacts with tubulin. Thus, CUR disrupts microtubule assembly, leading to cell cycle arrest in the mitotic phase in breast and cervical carcinoma cells; in MCF-7 cells, it disrupts the structure of the mitotic spindle, prevents normal anaphase movements, and leads to micronuclei (59, 60). An important aspect of the results obtained is that, for both actin and tubulin, the most pronounced morphological changes were observed with combined treatment. This finding is consistent with the rest of the experimental data — cell viability, general morphology, and apoptotic index - and suggests that the association between CIS and CUR amplifies cytoskeletal disruption.

Combined CIS and CUR treatment predominantly induces apoptosis in A375 cells

Given the results of the apoptotic index, the apoptotic/necrotic potential of treatment with CIS, CUR, and their combination was further investigated using

a double-staining assay with acridine orange and propidium iodide (AO/PI). The results (Figure 6) showed the presence of both apoptotic and necrotic cells following treatment with CIS and CUR, with effects more pronounced with the combination treatment. In the case of the combined treatment, a decrease in green fluorescence — corresponding to viable cells (AO-positive) — was observed, accompanied by morphological features of apoptosis such as cell rounding and chromatin condensation. Concurrently, an increase in the number of cells exhibiting red/orange fluorescence (PI-positive) was noted, indicating loss of membrane integrity consistent with late apoptotic and necrotic cell death.

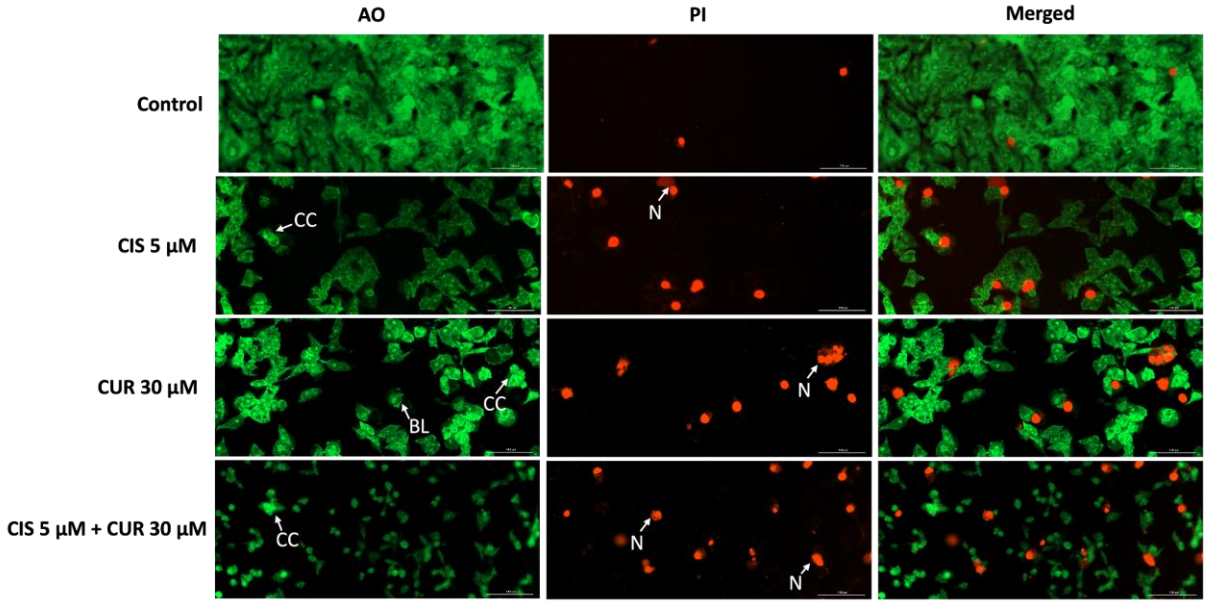

Figure 6.
Representative images of the impact of CIS, CUR, and a combination of the two compounds after 24 h in A375 cells stained with AO/PI. The scale bar indicates 100 µm. CC: chromatin condensation, BL: blebbing, N: necrotic/late apoptotic cells

Dual AO/PI staining is a fluorescence-based technique used extensively to assess cell viability and differentiate among various types of cell death, including apoptosis and necrosis. Acridine orange (AO) can penetrate intact cell membranes and bind to nucleic acids, generating green fluorescence in viable cells. Conversely, propidium iodide (PI) is repelled by intact membranes and can only permeate cells with impaired membrane integrity, where it emits red fluorescence after interacting with nucleic acids. This double-staining technique enables distinction among viable, apoptotic, and necrotic cells (20).

The results obtained in this study are consistent with the mechanism of cell death suggested by the apoptotic index and the previously analyzed changes at the nuclear and cytoskeletal levels. The decrease in the proportion of viable, AO-positive cells following treatment, together with the appearance of cell rounding and chromatin condensation, indicates that both CIS and CUR induced A375 cell death, an effect that was clearly amplified when the two compounds were combined. It should be noted that propidium iodide is incorporated not only by necrotic cells, but also by those undergoing late apoptosis, whose membrane integrity is ultimately compromised; therefore, the increase in red/orange fluorescence observed in the case of the combined treatment most likely reflects a combination of late apoptotic and necrotic events, rather than necrosis *per se* (39). This interpretation is in agreement with the predominantly apoptotic profile indicated by the apoptotic index and the characteristic morphological signs observed in the present study.

The coexistence of apoptotic and necrotic cells is a frequently reported phenomenon in *in vitro* cytotoxicity studies, especially under intense cytotoxic conditions. Thus, a portion of apoptotic cells that are not removed by phagocytosis may progress to secondary necrosis. This may explain the presence of the necrotic component alongside the apoptotic one, especially in the case of combined treatment, where cell viability was most reduced (61). Overall, these results indicate that the association between CIS and CUR induces the death of A375 melanoma cells through a predominantly apoptotic mechanism, accompanied by a secondary necrotic component, the overall effect exceeding that of the agents administered individually (62). These results are consistent with previous reports showing that CUR can

enhance the cytotoxic and pro-apoptotic activity of CIS across various tumor models, supporting the potential of this association as a chemosensitization strategy in melanoma.

Although these results are promising, particularly about combination therapy, the present study nevertheless has several limitations, including the assessment of treatment effects only after 24 hours, the need to investigate longer exposure periods (48 and 72 hours) and additional concentration ranges, as well as testing on other 2D and 3D melanoma models and animal models. Furthermore, the safety profile of the combination therapy should also be evaluated in healthy cell models. Therefore, future research directions should focus on addressing these limitations and further investigating how natural compounds, such as CUR, could be integrated into melanoma treatment protocols alongside other anticancer agents to improve the pharmacological profile of these treatments.

Conclusions

Skin cancers, including melanoma, remain among the most serious challenges in the medical field worldwide. Although conventional therapies provide promising results in the management of this disease, they are often associated with safety-related limitations. In this context, natural compounds have emerged as potential adjuvants to conventional anticancer therapies. In the present study, the combination of CIS and CUR demonstrated synergistic effects at the highest concentration tested *in vitro* on the A375 cell line, compared with the individual treatments. The results indicated a more pronounced decrease in cell viability and mitochondrial membrane potential, along with changes in several cellular components, such as nuclei, mitochondria, F-actin, and tubulin. The combination treatment also led to higher levels of apoptotic and necrotic cells than the individual treatments. That's why more extensive studies are needed to better understand the mechanism of action behind this combination and to explore its potential use in clinical practice.

Acknowledgement

The authors would like to thank "Victor Babeș" University of Medicine and Pharmacy Timișoara for supporting the experimental activities conducted in this study.

Funding

Not applicable.

Availability of data and materials

The data generated in the present study are included in the figures and/or tables of this article.

Ethics approval and consent to participate

Not applicable.

AI use disclosure

During the preparation of this manuscript, the authors used QuillBot for language improvement, including spelling, grammar, clarity, and readability. The authors reviewed and revised all outputs from these tools and take full responsibility for the final content of the work.

Conflict of interest

The authors declare no conflict of interest.

References

1. D'Arino A, Caputo S, Eibenschutz L, Piemonte P, Buccini P, Frascione P, et al. Skin cancer microenvironment: What we can learn from skin aging?. Int J Mol Sci. 2023;24(18):14043.
2. Parker ER. The influence of climate change on skin cancer incidence - A review of the evidence. Int J Womens Dermatol. 2020;7(1):17-27.
3. Spanos S, Singh N, Laginha BI, Arnolda G, Wilkinson D, Smith AL, et al. Measuring the quality of skin cancer management in primary care: A scoping review. Australas J Dermatol. 2023;64(2):177-193.
4. Zhou L, Zhong Y, Han L, Xie Y, Wan M. Global, regional, and national trends in the burden of melanoma and non-melanoma skin cancer: Insights from the global burden of disease study 1990-2021. Sci Rep. 2025;15(1):5996.
5. Slominski RM, Sarna T, Płonka PM, Raman C, Brożyna AA, Slominski AT. Melanoma, melanin, and melanogenesis: The yin and yang relationship. Front Oncol. 2022;12:842496.
6. Zeng L, Gowda BHJ, Ahmed MG, Abourehab MAS, Chen ZS, Zhang C, et al. Advancements in nanoparticle-based treatment approaches for skin cancer therapy. Mol Cancer. 2023;22(1):10.
7. Nurgali K, Jagoe RT, Abalo R. Editorial: Adverse effects of cancer chemotherapy: Anything new to improve tolerance and reduce sequelae?. Front Pharmacol. 2018;9:245.
8. Dehelean CA, Marcovici I, Soica C, Mioc M, Coricovac D, Iurciuc S, et al. Plant-derived anticancer compounds as new perspectives in drug discovery and alternative therapy. Molecules. 2021;26(4):1109.
9. Hasan N, Nadaf A, Imran M, Jiba U, Sheikh A, Almalki WH, et al. Skin cancer: Understanding the journey of transformation from conventional to advanced treatment approaches. Mol Cancer. 2023;22(1):168.
10. Hashemi M, Heshmatzad K, Shahsavan G, Tavakolpour V, Komeilie Esfahani S, Karimi P, et al. Natural bioactive molecules and chemotherapeutics synergism for enhanced cancer therapy. Nutr Metab (Lond). 2026;23(1):38.
11. Hewlings SJ, Kalman DS. Curcumin: A review of its effects on human health. Foods. 2017;6(10):92.
12. Moon DO. Curcumin in cancer and inflammation: An in-depth exploration of molecular interactions,

therapeutic potentials, and the role in disease management. Int J Mol Sci. 2024;25(5):2911.
13. Ghosh S. Cisplatin: The first metal based anticancer drug. Bioorg Chem. 2019;88:102925.
14. Karwaciak I, Sałkowska A, Karaś K, Dastych J, Ratajewski M. Targeting SIRT2 sensitizes melanoma cells to cisplatin via an EGFR-dependent mechanism. Int J Mol Sci. 2021;22(9):5034.
15. Piccioni M, Caputo E, Cuciniello R, Meo FD, Valentino A, Petillo G, et al. Curcumin impacts on cisplatin sensitivity determining apoptotic boost in mesothelioma. Biomed Pharmacother. 2025;193:118827.
16. Chou TC. Drug combination studies and their synergy quantification using the Chou-Talalay method. Cancer Res. 2010;70(2):440-446.
17. Talpos S, Chioran D, Alexandru GC, Dinu Ș, Coricovac ED, Smeu A, et al. Silibinin triggers mitochondrial apoptosis and declines clonogenic potential in Detroit 562 human pharyngeal carcinoma cells. Medicina (Kaunas). 2025;61(12):2197.
18. Dan C, Almajan-Guta B, Jojić AA, Dumitrel ȘI, Predescu IA, Tchiakpean-Tal D, et al. Ethanolic extract of *Juniperus communis* exhibits antimicrobial activity and selective cytotoxicity in PANC-1 cancer cells compared to HepaRG hepatocytes. Farmacia. 2025;73(2):362-370.
19. Marcovici I, Chioibas R, Zupko I, Pinzaru I, Moaca A, Ledeti A, et al. Preclinical pharmaco-toxicological screening of biomimetic melanin-like nanoparticles as a potential therapeutic strategy for cutaneous melanoma. Front Pharmacol. 2025;16:1487854.
20. Dahma R, Motoc M, Dumitrel ȘI, Haj Ali D, Morariu-Briciu DM, Bonțe D, et al. Digoxin exhibits anticancer activity in A375 and RPMI7951 cutaneous melanoma cells: a drug repurposing approach. Farmacia. 2025;73(5):1306.
21. Mitra A, Ghosh R. A375 melanoma cells are sensitized to cisplatin-induced toxicity by a synthetic nitro-flavone derivative 2-(4-nitrophenyl)-4H-chromen-4-one through inhibition of PARP1. Mol Biol Rep. 2021;48(8):5993-6005.
22. Muscella A, Cossa LG, Stefàno E, Rovito G, Benedetti M, Fanizzi FP, et al. Different cytotoxic effects of cisplatin on pancreatic ductal adenocarcinoma cell lines. Int J Mol Sci. 2024;25(24):13662.
23. Hu S, Xu Y, Meng L, Huang L, Sun H. Curcumin inhibits proliferation and promotes apoptosis of breast cancer cells. Exp Ther Med. 2018;16(2):1266-1272.
24. Kössler S, Nofziger C, Jakab M, Dossena S, Paulmichl M. Curcumin affects cell survival and cell volume regulation in human renal and intestinal cells. Toxicol. 2012;292(2-3):123-135.
25. Liston DR, Davis M. Clinically relevant concentrations of anticancer drugs: A guide for nonclinical studies. Clin Cancer Res. 2017;23(14):3489-3498.
26. Yu Y, Lee NY. JAVELIN Head and Neck 100: A phase III trial of avelumab and chemoradiation for locally advanced head and neck cancer. Future Oncol. 2019;15(7):687-694.
27. Schiborr C, Kocher A, Behnam D, Jandasek J, Toelstede S, Frank J. The oral bioavailability of curcumin from micronized powder and liquid micelles is significantly increased in healthy humans and differs between sexes. Mol Nutr Food Res. 2014;58(3):516-527.
28. Flory S, Sus N, Haas K, Jehle S, Kienhöfer E, Waehler R, et al. Increasing post-digestive solubility of curcumin is the most successful strategy to improve its oral bioavailability: A randomized cross-over trial in healthy adults and *in vitro* bioaccessibility experiments. Mol Nutr Food Res. 2021;65(24):e2100613.
29. Zhao G, Han X, Zheng S, Li Z, Sha Y, Ni J, et al. Curcumin induces autophagy, inhibits proliferation and invasion by downregulating AKT/mTOR signaling pathway in human melanoma cells. Oncol Rep. 2016;35(2):1065-1074.
30. Vaccaro F, Mannino F, Santarpia M, Cullotta C, Galeano M, Borgia F, et al. Genistein and curcumin inhibit proliferation and invasiveness in BRAFV600E mutant and wild-type melanoma cells: Insights into their anticancer effects. Biomedicines. 2025;13(8):1954.
31. Jamwal R. Bioavailable curcumin formulations: A review of pharmacokinetic studies in healthy volunteers. J Integr Med. 2018;16(6):367-374.
32. Liao W, Xiang W, Wang FF, Wang R, Ding Y. Curcumin inhibited growth of human melanoma A375 cells via inciting oxidative stress. Biomed Pharmacother. 2017;95:1177-1186.
33. Song L, McNeil EM, Ritchie AM, Astell KR, Gourley C, Melton DW. Melanoma cells replicate through chemotherapy by reducing levels of key homologous recombination protein RAD51 and increasing expression of translesion synthesis DNA polymerase ζ. BMC Cancer. 2017;17(1):864.
34. He Y, Zhu Q, Chen M, Huang Q, Wang W, Li Q, et al. The changing 50% inhibitory concentration (IC50) of cisplatin: A pilot study on the artifacts of the MTT assay and the precise measurement of density-dependent chemoresistance in ovarian cancer. Oncotarget. 2016;7(43):70803-70821.
35. Zhang W, Shi H, Chen C, Ren K, Xu Y, Liu X, et al. Curcumin enhances cisplatin sensitivity of human NSCLC cell lines through influencing Cu-Sp1-CTR1 regulatory loop. Phytomedicine. 2018;48:51-61.
36. Cho MK, Lee Y, Kim KD, Choi MH, Lee SH, Choi D, et al. Dietary polyphenols curcumin and resveratrol exert selective anticancer effects in melanoma cells. Nutrients. 2026;18:548.
37. Doonan F, Cotter TG. Morphological assessment of apoptosis. Methods. 2008;44(3):200-204.
38. Taatjes DJ, Sobel BE, Budd RC. Morphological and cytochemical determination of cell death by apoptosis. Histochem Cell Biol. 2008;129(1):33-43.
39. Costigan A, Hollville E, Martin SJ. Discriminating between apoptosis, necrosis, necroptosis, and ferroptosis by microscopy and flow cytometry. Curr Protoc. 2023;3(12):e951.
40. Carneiro MLB, Porfirio EP, Otake AH, Chammas R, Bao SN, Guillo LA. Morphological alterations and G0/G1 cell cycle arrest induced by curcumin in human SK-MEL-37 melanoma cells. Braz Arch Biol Technol. 2010;53(2):343-352.
41. Muhammed Y, Lazenby RA. Scanning ion conductance microscopy revealed cisplatin-induced morphological changes related to apoptosis in single adenocarcinoma cells. Anal Methods. 2024;16(4):503-514.
42. Wang Y, Rishi AK, Wu W, Polin L, Sharma S, Levi E, et al. Curcumin suppresses growth of mesothelioma

cells *in vitro* and *in vivo*, in part, by stimulating apoptosis. Mol Cell Biochem. 2011;357(1-2):83-94.
43. Reed JC, Kroemer G. Mechanisms of mitochondrial membrane permeabilization. Cell Death Differ. 2000;7(12):1145.
44. Sivandzade F, Bhalerao A, Cucullo L. Analysis of the mitochondrial membrane potential using the cationic JC-1 dye as a sensitive fluorescent probe. Bio Protoc. 2019;9(1):e3128.
45. Predescu IA, Boru C, Smeu A, Coricovac ED, Hoinoiu B, Tănase A, et al. Curcumin enhances cisplatin-induced cytotoxicity in PANC-1 and MIA PaCa-2 pancreatic cancer cells. Farmacia. 2026;74(1):78-92.
46. Kocyigit A, Guler EM. Curcumin induce DNA damage and apoptosis through generation of reactive oxygen species and reducing mitochondrial membrane potential in melanoma cancer cells. Cell Mol Biol (Noisy-le-grand). 2017;63(11):97-105.
47. Qiu Y, Yu T, Wang W, Pan K, Shi D, Sun H. Curcumin-induced melanoma cell death is associated with mitochondrial permeability transition pore (mPTP) opening. Biochem Biophys Res Commun. 2014;448(1):15-21.
48. Liga S, Tămaș A, Vodă R, Rusu G, Bîtcan I, Socoliuc V, et al. Puerarin-loaded proniosomal gel: Formulation, characterization, *in vitro* antimelanoma cytotoxic potential, and *in ovo* irritation assessment. Gels. 2026;12(1):72.
49. Bock FJ, Tait SWG. Mitochondria as multifaceted regulators of cell death. Nat Rev Mol Cell Biol. 2020;21(2):85-100.
50. Suen DF, Norris KL, Youle RJ. Mitochondrial dynamics and apoptosis. Genes Dev. 2008;22(12):1577-1590.
51. Sheridan C, Martin SJ. Mitochondrial fission/fusion dynamics and apoptosis. Mitochondrion. 2010;10(6):640-648.
52. Lee YJ, Jeong SY, Karbowski M, Smith CL, Youle RJ. Roles of the mammalian mitochondrial fission and fusion mediators Fis1, Drp1, and Opa1 in apoptosis. Mol Biol Cell. 2004;15(11):5001-5011.
53. Yu R, Lendahl U, Nistér M, Zhao J. Regulation of mammalian mitochondrial dynamics: Opportunities and challenges. Front Endocrinol (Lausanne). 2020;11:374.
54. Chazotte B. Labeling mitochondria with MitoTracker dyes. Cold Spring Harb Protoc. 2011;2011(8):990-992.
55. Desouza M, Gunning PW, Stehn JR. The actin cytoskeleton as a sensor and mediator of apoptosis. Bioarchitecture. 2012;2(3):75-87.
56. Maksimovich NYe, Bon EI, Portonenko AM. Cell death: Morphofunctional features. Biomed J Sci Tech Res. 2019;48(5):40181-40187.
57. Povea-Cabello S, Oropesa-Ávila M, de la Cruz-Ojeda P, Villanueva-Paz M, de la Mata M, Suárez-Rivero JM, et al. Dynamic reorganization of the cytoskeleton during apoptosis: The two coffins hypothesis. Int J Mol Sci. 2017;18(11):2393.
58. Zhou GZ, Cao FK, Du SW. The apoptotic pathways in the curcumin analog MHMD-induced lung cancer cell death and the essential role of actin polymerization during apoptosis. Biomed Pharmacother. 2015;71:128-134.
59. Jackson SJT, Murphy LL, Venema RC, Singletary KW, Young AJ. Curcumin binds tubulin, induces mitotic catastrophe, and impedes normal endothelial cell proliferation. Food Chem Toxicol. 2013;60:431-438.
60. Srivastava S, Mishra S, Surolia A, Panda D. C1, a highly potent novel curcumin derivative, binds to tubulin, disrupts microtubule network and induces apoptosis. Biosci Rep. 2016;36(2):e00323.
61. Silva MT. Secondary necrosis: The natural outcome of the complete apoptotic program. FEBS Lett. 2010;584(22):4491-4499.
62. Cacciola NA, Cuciniello RD, Petillo GD, Piccioni M, Filosa S, Crispi S. An overview of the enhanced effects of curcumin and chemotherapeutic agents in combined cancer treatments. Int J Mol Sci. 2023;24(16):12587.